HAL
open science

# Interdiffusion of Al and Ga in AlN/AlGaN superlattices grown by ammonia-assisted molecular beam epitaxy

M. Nemoz, F. Semond, S. Rennesson, M. Leroux, S. Bouchoule, G. Patriarche, J. Zuniga-Perez

## To cite this version:

M. Nemoz, F. Semond, S. Rennesson, M. Leroux, S. Bouchoule, et al.. Interdiffusion of Al and Ga in AlN/AlGaN superlattices grown by ammonia-assisted molecular beam epitaxy. Superlattices and Microstructures, 2021, 150, pp.106801. 10.1016/j.spmi.2020.106801 . hal-03357724

**HAL Id: hal-03357724**

**https://hal.science/hal-03357724**

Submitted on 29 Sep 2021

**HAL** is a multi-disciplinary open access archive for the deposit and dissemination of scientific research documents, whether they are published or not. The documents may come from teaching and research institutions in France or abroad, or from public or private research centers.

L'archive ouverte pluridisciplinaire **HAL**, est destinée au dépôt et à la diffusion de documents scientifiques de niveau recherche, publiés ou non, émanant des établissements d'enseignement et de recherche français ou étrangers, des laboratoires publics ou privés.

# Interdiffusion of Al and Ga in AlN/AlGaN superlattices grown by ammonia-assisted molecular beam epitaxy

M. Nemoz[1]*, F. Semond[1], S. Rennesson[1], M. Leroux[1], S. Bouchoule[2], G. Patriarche[2], J. Zuniga-Perez[1]
[1]*Université Côte d'Azur, CNRS, CRHEA, F-06560 Valbonne, France*
[2]*Centre de Nanosciences et de Nanotechnologies, CNRS, Univ. Paris-Sud, Université Paris-Saclay, F-91460 Marcoussis, France*
*Email: mn@crhea.cnrs.fr

## Abstract

Diffusion at the AlN/$Al_{0.3}Ga_{0.7}N$ interface was investigated by X-ray diffraction, high-angle annular dark field scanning transmission electron microscopy and energy-dispersive X-ray spectroscopy. AlN/$Al_{0.3}Ga_{0.7}N$ superlattices (SLs) have been grown at 800 °C on (111) silicon substrates by ammonia-assisted molecular beam epitaxy. Annealings on a 5-pair SL, carried out at the growth temperature in an ammonia-based atmosphere from 1h to 115h, show the occurrence of a diffusion process illustrated by the increase of the interface layer thickness. The cation interdiffusion is found to be weakly concentration-dependent while it seems to be more strain-dependent. The mean diffusion coefficient value determined in this study at the AlN/$Al_{0.3}Ga_{0.7}N$ interface is about $6\times10^{-18}$ $cm^2/s$ at the growth temperature. The effect of the unintentional annealing of buried layers during long growth runs is exemplified on a 45-pair SL. The measurement of the actual composition profile along the growth direction shows the formation of an unintentional AlGaN graded layer of intermediate composition at each interface. The thickness of each of these interfacial layers is found to decrease along the SL growth direction, pointing towards the influence of the overall time spent at growth temperature as a determining parameter.

**Keywords:** B1. Nitrides; B2. Semiconducting III-V materials; A3. Molecular beam epitaxy; A1. Diffusion; A1. High resolution X-ray diffraction

# 1. Introduction

The presence of an unintentional interface layer has been reported for thick AlGaN layers grown by metalorganic chemical vapor deposition (MOCVD) directly on sapphire substrate [1,2] or on various nitride layers [3]. Such interface layers have also been observed in AlN/AlGaN Distributed Bragg Reflectors (DBRs) grown by plasma assisted molecular beam epitaxy (PA-MBE) [4] and MOCVD [5,6]. The presence of these unintentional interface layers was attributed to the stress-induced composition pulling effect.

Chemical diffusion is another well-known phenomenon that can lead to an interface layer. So far few studies have dealt with cation interdiffusion in the GaN/AlN system: during MOCVD growth at 1100 °C [7] and after annealing at temperatures going from 1000 °C to 1700 °C [8–10]. Based on these studies a set of diffusion coefficients were reported in the literature, but the estimated values spread over a wide range and are not consistent with each other, even if their temperature dependence is taken into account. In $Al_{0.03}Ga_{0.97}N$/AlN superlattices (SLs) a $D$ value of $7\times10^{-20}$ $cm^2/s$ has been reported at 1000 °C [8] and a $D$ value of $1.3\times10^{-17}$ $cm^2/s$ has been extracted from experiments in $Al_{0.06}Ga_{0.94}N$/GaN quantum well structures annealed at 1500 °C [9]. While a $D$ value as high as $10^{-14}$ $cm^2/s$ has been determined for $Al_{0.02}Ga_{0.98}N$/GaN and AlN/GaN structures annealed at 1100 °C [7].

X-ray diffraction (XRD) is very sensitive to the structure and the chemical composition of the materials. Moreover, SLs have two advantages for studying interdiffusion using XRD: the first is obviously the increase of the intensity diffracted by the set of interface layers compared to a single interface; the second is related to the characteristic shape of the SL XRD diagram. Indeed, for reflections along the growth axis, each reflection generates a periodic group of peaks named satellite peaks. The gap between two consecutive satellite peaks is determined by the thickness of the SL period, the position of the peak group is fixed by the SL strain and mean chemical composition, and the relative intensity of each satellite peak is determined by the chemical composition profile of the SL period. A single SL XRD diagram thus allows to dissociate several competing mechanisms potentially involved in the diffusion process.

In this work we show the appearance and evolution of the interface layer by studying a 5-pair AlN/AlGaN SL grown by $NH_3$-assisted MBE at 800 °C and subsequently annealed at the growth temperature in an ammonia-based atmosphere from 1 to 115 hours. The SL period composition profiles are determined by the simulation of the $2\theta$-$\omega$ scans of the (0002) symmetric reflection. The study of the variation of the composition profile with annealing enables to extract the interdiffusion coefficient of Al and Ga at the AlN/AlGaN interface at 800 °C. The variation of the concentration-dependent interdiffusion coefficient with the annealing time seems to indicate that the interdiffusion process is mostly strain-dependent. Then we illustrate the importance of the interdiffusion occurring at growth temperature on a functional structure: a DBR made of 45 pairs of AlN/AlGaN grown by $NH_3$-assisted MBE at 800 °C and whose growth lasts about 24 hours. The DBR period composition profile as well as its variation along the growth axis are determined by XRD and high-angle annular dark field (HAADF) scanning transmission electron microscopy (STEM) coupled to energy-dispersive X-ray spectroscopy (EDX) analysis. The variation of the composition profile along the growth axis clearly demonstrates the impact of the unintentional annealing of the buried DBR layers during the growth of the following pairs.

## 2. Experimental procedure

The $(AlN/Al_{0.3}Ga_{0.7}N)_5$ SL structure was grown on (111) silicon substrate at 800 °C by $NH_3$-MBE in a Riber Compact 21 growth reactor. Targeted thicknesses of AlN and $Al_{0.3}Ga_{0.7}N$ layers were 42 and 37 nm respectively. The total growth duration of the 5-pair SL was about 3 hours. Then the 5-pair SL was annealed in the MBE reactor from 1 to 115 hours. The annealing conditions are the same as those used when growing the SL: at 800 °C and under an ammonia equivalent pressure of $10^{-5}$ Torr. After each annealing the sample was studied by XRD. The $(AlN/Al_{0.3}Ga_{0.7}N)_{45}$ DBR structure was grown under the same growth conditions than the 5-pair SL structure, keeping the same layer thicknesses and Al content. In order to avoid the formation of cracks, the epitaxy was performed on silicon substrates structured in 400x400 $\mu m^2$ mesas [11]. The epitaxial structure consists in a 300 nm AlN buffer layer, followed by 45 pairs of AlN and $Al_{0.3}Ga_{0.7}N$ layers grown at 800 °C, and ended by a 400 nm-thick GaN

optical cavity. The total growth duration of the 45-pair DBR is about 24 hours. The threading dislocation densities determined at the surface of the stack by atomic force microscopy (resp. on plane view STEM images) are in the range of $1.10^{10}$ $cm^{-2}$ (resp. $3.10^{10}$ $cm^{-2}$). From cross-sectional STEM images the dislocation density at the bottom of the structure can be estimated about 5 times higher.

The aluminum content profiles are determined from $2\theta$-$\omega$ scans of the (0002) symmetric reflection measured with an analyzer crystal before the detector in a Malvern Panalytical X'Pert PRO MRD four-circle diffractometer. These scans have been simulated with the Malvern Panalytical Epitaxy software. X-ray reciprocal space maps of the $(20\bar{2}4)$ asymmetric reflection have been recorded without analyzer because of the low diffracted intensities.

Interface layers have been also observed by HAADF maps: STEM lamellas were prepared using focused ion beam (FIB) etching from the $(AlN/Al_{0.3}Ga_{0.7}N)_{45}$ DBR. STEM/TEM cross-sectional observations coupled to EDX analysis were performed with a FEI Titan Themis 200 microscope equipped with an aberration corrector on the probe (STEM mode), and a Super-X windowless four-quadrant silicon-drift EDX detector with a solid angle larger than 0.7 srad. The spatial resolution of the EDX point measurement is about 2 nm. In the atomic percentages calculations, the Cliff-Lorimer model for the correction of the absorption was used, and the k-factors of the $K_\alpha$ emission lines were fixed from separate measurements on thick epitaxial AlN and GaN standard samples. The STEM lamella thickness was fixed to its nominal value of (80 ± 10) nm, and the material average density was fixed to (5 ± 1) $g/cm^{-3}$. The corresponding uncertainty in the calculated Al% is estimated to be between ±1% and ±2.5% for Al contents close to 100% and 30%, respectively.

# 3. Results and discussion

## 3.1. Characterization of the diffusion process

### 3.1.1. Interface layer evolution

The development of a graded interface during the annealing of the $(AlN/Al_{0.3}Ga_{0.7}N)_5$ structure is clearly visible on the X-ray reciprocal space maps of the $(20\bar{2}4)$ reflection, which have been recorded systematically for a series of annealing durations (Fig. 1). The "AG" sample corresponds to the as-grown sample and the "*n*h" samples correspond to this 5-pair SL after *n* hours of annealing. The symmetry of the structure imposes biaxial strain, which enables to extract Al content values in the AlGaN alloys considering the strain relation $\varepsilon_{zz} = -2\varepsilon_{xx}\, C_{13}/C_{33}$ and using Vegard's law. The stiffness coefficients $C_{13}$ and $C_{33}$ used are those calculated by Wright and *al.* [12]. The highest (resp. lowest) $Q_Z$ peak in the maps correspond to AlN (resp. $Al_{0.32}Ga_{0.68}N$), while the intermediate peak has to be attributed to a graded layer appearing during annealing. Clearly, after each annealing the graded layer intensity increases, indicating an increase of its thickness. At the same time, the mean $Q_Z$ value of the graded layer decreases with annealing time, showing a mean Al content varying from about 80% after 4 hours of annealing to about 65% after a 115 hours anneal.

### 3.1.2. Al content profile

To follow up quantitatively the evolution of the interface layer composition profile with the annealing duration, the $2\theta$-$\omega$ scan of the (0002) reflection was measured and simulated for each annealing duration. For the sake of clarity, Fig. 2(a) presents only the measured $2\theta$-$\omega$ scans for the as-grown sample (blue line), the 14-hour (green line) and the 115-hour (red line) annealing with the corresponding simulations (black lines). The period thickness $\Lambda$ = 82.3 nm determined from these simulations does not vary upon annealing. The deduced period composition profiles of the as-grown and of all the annealed samples are shown in Fig. 2(b). The AlGaN layer contains 32% of Al and the AlN layer is a pure binary as previously measured on the $(20\bar{2}4)$ RSMs. The shape of the composition profile presents two discontinuities at the borders of the interface layer. While these discontinuities are not expected within a standard diffusion picture, they represent the linear fits giving the smallest standard deviations for all our samples. Besides, they are consistent with the EDX analysis of the 45-pair sample

discussed further, which shows an abrupt change in the slope of the composition gradient. It is noticeable that the AlN layer thickness decreases faster than that of the AlGaN layer during the annealings.

The thicknesses of the three layers building each SL period, deduced from the fits are presented in Fig. 2(c) as a function of annealing duration. The AlGaN (resp. AlN) layer thickness variation has been fitted (dotted line) with an exponential curve decreasing asymptotically towards 21 nm (resp. 12 nm). Note that the logarithmic fit (red dotted line) of the interface layer thickness falls down to zero at about -3 h, suggesting that a non-vanishing interface layer thickness exists just after the growth of each AlN/AlGaN pair.

### 3.1.3. Diffusion coefficient

Few studies have been done to determine the cation interdiffusion coefficient values in the GaN/AlN system. To our knowledge, all these works use the concentration-independent interdiffusion approximation. The diffusion coefficient can be determined from Fick's second law:

$$\frac{\partial C}{\partial t} = \nabla(D\nabla C). \tag{1}$$

If we consider that the diffusion coefficient $D(T)$ depends only on the temperature, then the composition profile can be written as an error function and the diffusion length $L_D$ is defined as [13]:

$$L_D^2 = 4D(T)t + L_{D_0}^2, \tag{2}$$

where $t$ is the annealing duration and $L_{D_0}$ is the initial interface layer thickness, obtained from the intercept at $t = 0$.

From our profile we can estimate the diffusion length $L_D$ as half of the interface layer thickness. The squared diffusion length against the annealing duration is plotted in Fig. 3(a): as the trend is not linear, we cannot determine a unique value of the diffusion coefficient at 800 °C. Until 4 hours of annealing, the $D$ value is at $(8.3\pm2.4)10^{-18}$ cm².s$^{-1}$ (red dashed straight line), whereas between 40 and 115 hours of annealing the extracted $D$ value decreases to about $(2.3\pm0.9)10^{-18}$ cm².s$^{-1}$ (blue dashed straight line).

Therefore, the diffusion coefficient in this AlN/$Al_{0.3}Ga_{0.7}N$ SL does not only depend on the temperature. If the chemical composition during diffusion varies over a certain concentration range, then diffusing particles will experience different chemical environments and hence different diffusion coefficients. Thus, the diffusion coefficient can also be concentration dependent [14]. Fick's second law for interdiffusion in one dimension can be written then as:

$$\frac{\partial C}{\partial t} = D(T,C)\frac{\partial^2 C}{\partial z^2} + \frac{dD\,(T,C)}{dc}\left(\frac{\partial C}{\partial z}\right)^2, \tag{3}$$

with $D(T,C) = D_0(T)e^{\alpha(T)C}$, where $C$ is the Al concentration. Consequently, at $T$ = 800 °C, $D_0$ is the diffusion coefficient of Al in pure GaN and $D_0\, e^{\alpha}$ that of Ga in pure AlN.

At a given temperature, Eq. (3) becomes:

$$\frac{\partial C}{\partial t} = D_0 e^{\alpha C}\left[\frac{\partial^2 C}{\partial z^2} + \alpha\left(\frac{\partial C}{\partial z}\right)^2\right]. \tag{4}$$

This equation was integrated numerically using $\frac{\partial f}{\partial t} \approx \frac{f(t+\Delta t)-f(t)}{\Delta t}$ with $\Delta z$ = 0.5 nm and $\Delta t$ = 2 min. Figure 3(b) compares the XRD composition profiles (continuous lines) and the numerical solutions of Eq. (4) (dashed lines) for two $D_0$ values. For the purpose of comparison, the composition profiles of Fig. 2(b) are represented in Fig. 3(b) by their best sigmoidal fits. For the sake of clarity, only the as-grown and the 4h, 14h, 40h, 115h samples are presented. The $\alpha$ value is 0.2 for both cases to fit the position of the highest slope; this positive $\alpha$ value means that the $Ga^{3+}$ cations diffuse faster in the AlN layer than the $Al^{3+}$ cations in the AlGaN layer. Therefore the diffusion activation energy seems lower for $Ga^{3+}$ than for $Al^{3+}$ in wurtzite nitride structures, which might be related to the stiffest bonds of AlN compared to GaN. The concentration-independent interdiffusion approximation is acceptable in view of the low concentration dependence found in this work. Indeed, the $\alpha$ value of 0.2 obtained for our AlN/AlGaN SL at 800 °C is low compared to the one found in GaAs/AlAs multilayers [15] of 2.06 at 860 °C, pointing towards a smaller chemical composition dependence of the diffusion coefficient in the AlN/AlGaN system than in the GaAs/AlAs one. The diffusion coefficient values $D$ reported in the literature for the GaN/AlN system spread over a wide range, from $7\times10^{-20}$ to $10^{-14}$ $cm^2/s$, and are not consistent with each other, even if the temperature dependence is taken into account. In our work, the mean $D$ value is about

$6\times10^{-18}$ cm$^2$/s for AlN/$Al_{0.3}Ga_{0.7}N$ SL. Indeed, for $D_0 = 4.5x10^{-18}$ cm².s$^{-1}$ (top graph on Figure 3(b)) the interface layer profile is well fitted for the 115h annealing time but not for the other annealing durations. In the same way, for $D_0 = 8.2x10^{-18}$ cm².s$^{-1}$ (bottom graph on Figure 3(b)) the best fit of the composition profile is obtained for the 4-hours annealing time. The different $D_0$ values obtained after 4 hours and 115 hours of annealing might mean that the diffusion is not only temperature and chemical concentration dependent.

The atomic mechanisms of diffusion in semiconductors are closely connected with defects. For GaAs based materials it has been shown that the diffusion is controlled by the concentration of vacancies [15–19]. In GaN based materials, the effect of linear defects, namely dislocations, on the diffusion process has also to be taken into account. The diffusion path of an atom in nitrides combines slow diffusion processes via vacancies and short circuit processes via dislocations [9]. Even if it is generally accepted that the strain can affect the crystal point defect density, the relation between strain and vacancy density in nitrides is not well known. It has been theoretically predicted that the cation vacancy formation energy should weakly decrease in GaN and AlN when applying a hydrostatic pressure [20], but the result under epitaxial strain could be different. The dislocation density evolution with strain has been the object of numerous studies and annealing is widely used to reduce the dislocation densities in AlN thin films [21–23].

### 3.1.4. Strain evolution

To evaluate if the interdiffusion is linked to the strain variation, the mean *a* lattice parameter has been determined as a function of annealing duration. The *a* value of the 115h sample was extracted from the $(20\bar{2}4)$ reciprocal space map recorded with a crystal analyzer. As the other RSMs were recorded without a crystal analyzer, the *a* values determined from these RSMs are not accurate enough. Therefore, considering a biaxial strain, the *a* lattice parameter values was determined from:

$$a = a_{115h}\left(1 + \frac{C_{33}}{2C_{13}}\varepsilon_c\right), \quad (5)$$

where $a_{115h}$ is the in-plane lattice parameter of the 115h sample, $C_{13}$ and $C_{33}$ are the stiffness coefficients of the $Al_{0.69}Ga_{0.31}N$ alloy corresponding to the SL mean composition. $\varepsilon_c$ is the out-of-plane deformation relative to the 115h sample and it is the opposite to the relative variation of the reciprocal vector $Q$ determined from the most intense peak of the SL (0002) reflection (34.9°<2θ<35.0° in Fig. 2(a)). Importantly, the $Q$ value only depends on the strain if the mean composition of the SL does not change after the annealing, which is the actual situation.

Due to the thermal coefficients mismatch between nitrides and silicon, GaN and AlN layers grown on (111) silicon substrates undergo a tensile stress at room temperature after the cooling down from growth temperature [24–26]. Besides, grain coalescence during the early growth stages already introduces a tensile stress contribution [27,28]. This can explain the mean tensile strain (averaged over the whole SL) measured on the as-grown 5-pair SL (Fig. 4), even if the AlN and AlGaN layers are individually in tensile and compressive strain, respectively. Indeed, the in-plane lattice parameter of the SL equivalent alloy fully relaxed at growth temperature, and then tensely strained by the silicon substrate during the cooling down, is $a$ ($Al_{0.69}Ga_{0.31}N$) = 3.142 Å at room temperature (see Table I). More in detail: first a drastic drop can be seen between the as-grown sample value and the 1h-annealed one (black dashed straight line). From then on, the in-plane lattice parameter variation can be fitted (red dashed line) with an exponential curve decreasing asymptotically towards 3.1445 Å, which corresponds to the 115h-annealing value. It is noticeable that this in-plane lattice parameter value is just slightly higher than that of the SL equivalent alloy fully relaxed at growth temperature, which seems to point towards a relationship between the overall strain and the interdiffusion process. Taking into account the thermal expansion coefficient of silicon, the 5-pair SL mean in-plane lattice parameter value varies, at 800 °C, from 3.157 Å after growth to 3.152 Å after the 115-hour annealing (see Table I), corresponding to a decrease of the mean tensile strain from 0.24% to 0.08%. In the same time, the diffusion coefficient decreases by about 50%.

TABLE I. In-plane lattice parameter values, at the growth temperature and after the cooling down on the Si substrate, of the 5-pair AG and 115h samples, and the SL equivalent alloy fully relaxed at growth temperature.

| **a (Å)** | 5-pair SL<br>AG sample | 5-pair SL<br>115h sample | $Al_{.69}Ga_{.31}N$<br>relaxed at 800 °C |
|---|---|---|---|
| At 800 °C | 3.157 | 3.152 | 3.149 |
| At 25 °C | 3.150 | 3.144 | 3.142 |

It is important to note that by performing the annealing of the 5-pair $AlN/Al_{0.3}Ga_{0.7}N$ SL, we have shown that the interdiffusion of Al and Ga atoms occurs in this type of structure even at a temperature as low as 800 °C.

## 3.2. Interface layer in distributed Bragg reflectors

In this part, we illustrate the effect of the Al/Ga interdiffusion during the growth of a functional structure: a DBR made of 45 pairs of AlN/AlGaN grown by $NH_3$-assisted MBE at 800 °C during about 24 hours. This long growth duration leads to an unintentional annealing of the underlying pairs during the growth of the following pairs.

### 3.2.1. HAADF-STEM and EDX analysis

A general view of the $(AlN/Al_{0.3}Ga_{0.7}N)_{45}$ DBR is shown in Fig. 5(a), where the chemical contrast of the HAADF map enables to discriminate each individual DBR pair, as well as the bottom AlN buffer layer and the top GaN cavity layer. Interfaces seem sharper within the top pairs than within the bottom ones, which is confirmed in Figs. 5(b)-(c) at a larger magnification. Besides the abruptness of the interfaces, a HAADF map of the first periods grown on top of the buffer AlN layer (Fig. 5(b)) shows

that the interface layer, with the intermediate Al composition, is the thickest layer among those building each AlN/AlGaN pair. More accurately, a four-layers stacking can be observed on these first periods, with a thicker interface layer at the AlN-on-AlGaN interface and a thinner one at the AlGaN-on-AlN interface. On the other hand, the last periods of the DBR (Fig. 5(c)), i.e. those in contact with the GaN cavity, show a three-layers stacking with a thin interface layer at the AlN-on-AlGaN interface only, whereas the AlGaN-on-AlN interface is much sharper.

The fact that the interface layer after the AlGaN is thicker than that after the AlN can be explained by the segregation of Ga atoms at the growth surface [29], some of which stay on the surface and act as an excess Ga during the AlN layer growth, contributing to a thicker interface layer. The strain state difference at the bottom and the top of the AlN layers can also affect the diffusion. Indeed, the AlN bottom atomic monolayers are strained on the AlGaN layer whereas the AlN top atomic monolayers are more relaxed. As AlN has stiffest bonds compared to AlGaN, the AlN layers accumulate more strain and thus have more impact on the diffusion process.

The composition profiles of the bottom and top periods have been determined by EDX linescans parallel to the growth direction (Fig. 6). Averaged spot measurements have also been performed in the AlN buffer layer, and in the GaN cavity layer, exhibiting pure binary compositions. For an easier comparison, the EDX profiles of the 1$^{st}$ and 2$^{nd}$ (blue line) DBR periods as well as those of the 44$^{th}$ and 45$^{th}$ (red line) DBR periods have been superimposed in Fig. 6. The last two top periods of the DBR exhibit a quasi-step profile, whereas the first two bottom periods of the DBR show a thick interface layer at the AlN-on-AlGaN interface and a thin interface layer at the other one, as observed in the HAADF images. At the bottom periods, where the diffusion is maximum, the EDX profile shows the largest composition gradient slopes near the AlN and AlGaN interfaces, consistent with the discontinuous profiles determined with XRD. It can be noted that the Al content difference in the AlGaN layers between the bottom (~39%) and the top (~32%) periods is slightly higher than the Al content uncertainty and, therefore, meaningful.

### 3.2.2. X-ray diffraction

Figure 7(a) shows the $(20\bar{2}4)$ asymmetric reflection of the 45-pair DBR. The lowest $Q_z$ peak corresponds to the GaN cavity while the intensity of the AlN buffer peak is too low to be discriminated from the AlN DBR peaks. Two black crosses indicate the theoretical positions of bulk GaN and AlN reflections. The three aligned peaks in $Q_x$ come from the DBR and correspond to a mean in-plane lattice parameter value of (3.1460 ± 0.0015) Å at room temperature. The $Q_z$ values of these three peaks correspond to out-of-plane lattice parameters of 4.960 Å, 5.017 Å and 5.133 Å (± 0.002 Å) at room temperature. The biaxial strain relation enables to extract Al content values in the AlGaN alloys of 97.5%, 76.5% and 32.0% (± 1.5%) for AlN layer, the interface layer and the AlGaN layer, respectively.

Figure 7(b) shows the measured (black line) $2\theta$-$\omega$ scan of the (0002) reflection of this DBR: the lowest angle peak is the one of the GaN cavity layer, whereas all other peaks are typical satellites peaks of a superlattice and, therefore, originate from the $(AlN/Al_{0.3}Ga_{0.7}N)_{45}$ DBR. Again, the AlN buffer layer peak is too weak here to be seen and hidden by the superlattice peaks. The thickness of the SL period ($\Lambda$ = 76.8 nm) has been determined from the spacing between two consecutive satellite peaks. These peaks can be grouped into three classes: for $2\theta < 35.1°$ (resp. $2\theta > 36.0°$), the relative intensities are mainly influenced by the thickness and the composition of AlGaN (AlN) layer, while between these angles the simulated relative intensities depend mainly on the presence or absence of an interface layer in the modeled DBR. Figure 7(c) shows three simulated aluminum concentration profiles in the DBR period. The "step" profile (red line) is made of a 36.0 nm thick $Al_{0.32}Ga_{0.68}N$ (AlGaN) layer and a 40.8 nm thick $Al_{0.97}Ga_{0.03}N$ (AlN) layer, without any interface layer. The "1st SL" (resp. "2nd SL") profile, blue line (resp. dark yellow line), contains a 20 nm (resp. 40 nm) thick interface layer. It can be clearly seen in Fig. 7(b) that the absence of an interface layer results in relative peak intensities that are too low (red line), while much better agreement between simulation and experiment is obtained when introducing an interface layer (blue and green lines). However, if the interface layer employed in the simulation is the same along the entire DBR thickness, the simulated curve does not reproduce the double-peak structure clearly seen in several intermediate satellites (see blue curve in the insert of Fig. 7 (b)). In fact, the best fit is achieved when using two different interface layers (whose composition

profiles are shown in Fig. 7(c)) distributed as follows along the DBR growth direction: the first 1/5 DBR thickness is simulated employing the "2nd SL" (dark yellow concentration profile), with a mean *a* lattice parameter of 3.134 Å, while the last 4/5 DBR thickness is simulated employing the "1st SL" (blue concentration profile), with a mean *a* lattice parameter of 3.145 Å (see Table II). This indicates that both the strain and the concentration profile undergo a strong variation along the growth axis. Due to the strain state of each SL profile, we can associate the "2nd SL" to the bottom part of the DBR, directly deposited on the AlN buffer (which imposes a compressive strain on the layers deposited just on top of it). Interestingly, if we do such an association (solely based on the strain state), it turns out that the thickness of the interface layer is much larger (40 nm instead of 20 nm) for the first DBR pairs than for the last ones, consistent with the HAADF-STEM measurements described before.

The Al concentration profiles determined by EDX at the AlN/AlGaN interface of the 2nd and the 44th periods of the DBR are reported in Fig. 7(c) for comparison. EDX and XRD profiles have been determined independently and both exhibit the same shape. Obviously the interface layer of the "1st SL" XRD profile, representing the mean of the top 4/5 DBR thickness, is broader than that of the 44th period. It should be noted that the second interface layer seen on the HAADF maps at the AlGaN/AlN interface has been considered too in the XRD simulations, but clearly the (0002) reflection is not sensitive enough to this second interface layer and, thus, we have preferred to use only one in the simulations employed in this article.

TABLE II. Simulation parameters of the (0002) reflection of the 45-pair DBR with two superlattices (SL) in the entire DBR thickness (*t*).

| | DBR ratio | *a* (Å) | $t_{AlGaN}$ (nm) | $t_{interface\ layer}$ (nm) | $t_{AlN}$ (nm) |
|---|---|---|---|---|---|
| 1st SL | 4/5 | 3.145 | 30 | 20 | 26.8 |
| 2nd SL | 1/5 | 3.134 | 20 | 40 | 16.8 |

## 4. Conclusions

In this work we show that interdiffusion of Al and Ga occurs in AlN/$Al_{0.3}Ga_{0.7}N$ superlattices at a temperature as low as 800 °C. The evolution of the interface layer thickness under voluntary annealing shows that the cation interdiffusion is weakly concentration-dependent while it seems to be more strain-dependent. The mean diffusion coefficient value determined in this study at the AlN/$Al_{0.3}Ga_{0.7}N$ interface is about $6\times10^{-18}$ $cm^2/s$.

In practice, this interdiffusion process must be present in any produced sample whose growth requires more than several hours. To illustrate this fact, an AlN/$Al_{0.3}Ga_{0.7}N$ distributed Bragg reflector with 45 pairs have been analyzed, showing clearly that the unintentional annealing of buried layers during the long growth runs (typically lasting about 24 hours) increases the interface layer thickness even if grown at 800 °C. As the unintentional annealing duration is directly proportional to the position of the AlN/AlGaN pair within the DBR, the interface layer thickness decreases along the growth axis of the DBR.

This interface layer is probably present in other AlN/AlGaN structures and could be responsible of a degraded interface abruptness. In order to reduce the diffusion in the AlN/AlGaN system, further studies are needed to evaluate the flexibility of the growth conditions to reduce the temperature and growth time of the structures, as well as the duration of the layers above. Moreover, a fine strain management of the interfaces seems crucial to control one of the driving forces of the interdiffusion process. Reducing or eliminating this interface layer may be critical for some electronic or optoelectronic applications for which abrupt interfaces are required.

## Acknowledgements

This work was partially supported by ANR though project Plug-And-Bose (ANR-16-CE24-0021). C2N is a member of RENATECH (CNRS), the national network of large micro-nanofabrication facilities. The authors are pleased to thank B. Vinter for helpful discussion about numerical calculations.

## References


[1] Y.-L. Tsai, C.-L. Wang, P.-H. Lin, W.-T. Liao, J.-R. Gong, Appl. Phys. Lett. 82 (2003) 31–33.

[2] H.Y. Lin, Y.F. Chen, T.Y. Lin, C.F. Shih, K.S. Liu, N.C. Chen, J. Cryst. Growth. 290 (2006) 225–228.

[3] C. He, Z. Qin, F. Xu, L. Zhang, J. Wang, M. Hou, S. Zhang, X. Wang, W. Ge, B. Shen, Sci. Rep. 6 (2016) 25124.

[4] ž. Gačević, A. Eljarrat, F. Peiró, E. Calleja, J. Appl. Phys. 113 (2013) 183106.

[5] B. Liu, R. Zhang, J.G. Zheng, X.L. Ji, D.Y. Fu, Z.L. Xie, D.J. Chen, P. Chen, R.L. Jiang, Y.D. Zheng, Appl. Phys. Lett. 98 (2011) 261916.

[6] C.M. Wu, B.P. Zhang, J.Z. Shang, L.E. Cai, J.Y. Zhang, J.Z. Yu, Q.M. Wang, Semicond. Sci. Technol. 26 (2011) 055013.

[7] N. Chaaben, J. Laifi, H. Bouazizi, C. Saidi, A. Bchetnia, B. El Jani, Mater. Sci. Semicond. Process. 42 (2016) 359–363.

[8] J.J. Wierer, A.A. Allerman, E.J. Skogen, A. Tauke-Pedretti, G.A. Vawter, I. Montaño, Appl. Phys. Express. 8 (2015) 061004.

[9] S. Porowski, I. Grzegory, D. Kolesnikov, W. Lojkowski, V. Jager, W. Jager, V. Bogdanov, T. Suski, S. Krukowski, J. Phys. Condens. Matter. 14 (2002) 11097.

[10] C. Leclere, V. Fellmann, C. Bougerol, D. Cooper, B. Gayral, M.G. Proietti, H. Renevier, B. Daudin, J. Appl. Phys. 113 (2013) 034311.

[11] J. Zuniga-Perez, E. Mallet, R. Hahe, M.J. Rashid, S. Bouchoule, C. Brimont, P. Disseix, J.Y. Duboz, G. Gommé, T. Guillet, O. Jamadi, X. Lafosse, M. Leroux, J. Leymarie, F. Li, F. Réveret, F. Semond, Appl. Phys. Lett. 104 (2014) 241113.

[12] A.F. Wright, J. Appl. Phys. 82 (1997) 2833.

[13] J. Crank, Mathematics of Diffusion, Oxford, Clarendon, 1957.

[14] P. Heitjans, J. Kärger, Diffusion in Condensed Matter, Springer-Verlag, Berlin/Heidelberg, 2005.

[15] R.M. Fleming, D.B. McWhan, A.C. Gossard, W. Wiegmann, R.A. Logan, J. Appl. Phys. 51 (1980) 357–363.

[16] S. Ryu, I. Kim, B. Choe, W.G. Jeong, Appl. Phys. Lett. 67 (1995) 1417–1419.

[17] H. Bracht, E.E. Haller, K. Eberl, M. Cardona, Appl. Phys. Lett. 74 (1999) 49–51.

[18] W.P. Gillin, D.J. Dunstan, Comput. Mater. Sci. 11 (1998) 96–100.

[19] S.F. Wee, M.K. Chai, K.P. Homewood, W.P. Gillin, J. Appl. Phys. 82 (1997) 4842–4846.

[20] I. Gorczyca, N.E. Christensen, A. Svane, Phys. Rev. B. 66 (2002) 075210.

[21] M. Nemoz, R. Dagher, S. Matta, A. Michon, P. Vennéguès, J. Brault, J. Cryst. Growth. 461 (2017) 10–15.

[22] H. Miyake, G. Nishio, S. Suzuki, K. Hiramatsu, H. Fukuyama, J. Kaur, N. Kuwano, Appl. Phys. Express. 9 (2016) 025501.

[23] J.D. Greenlee, B. Gunning, B.N. Feigelson, T.J. Anderson, A.D. Koehler, K.D. Hobart, F.J. Kub, W.A. Doolittle, Electron. Mater. Lett. 12 (2016) 133–138.

[24] B.H. Bairamov, O. Gürdal, A. Botchkarev, H. Morkoç, G. Irmer, J. Monecke, Phys. Rev. B. 60 (1999) 16741.

[25] E. Feltin, B. Beaumont, M. Laügt, P. de Mierry, P. Vennéguès, H. Lahrèche, M. Leroux, P. Gibart, Appl. Phys. Lett. 79 (2001) 3230–3232.

[26] D.G. Zhao, S.J. Xu, M.H. Xie, S.Y. Tong, H. Yang, Appl. Phys. Lett. 83 (2003) 677–679.

[27] D. Magnfält, Dissertation, Linköping University, 2014.

[28] N. Mante, S. Rennesson, E. Frayssinet, L. Largeau, F. Semond, J.L. Rouvière, G. Feuillet, P. Vennéguès, J. Appl. Phys. 123 (2018) 215701.

[29] P. Boguslawski, K. Rapcewicz, J.J. Bernholc, Phys. Rev. B. 61 (2000) 10820.

# Figure captions

## Figure 1: single column

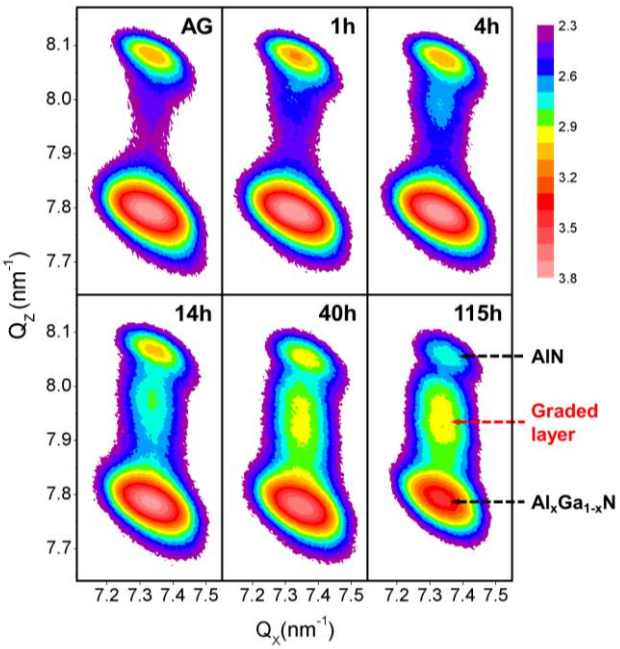


FIG. 1. X-ray reciprocal space maps of the $(20\bar{2}4)$ reflection of a 5-pair $AlN/Al_{0.3}Ga_{0.7}N$ superlattice: as-grown sample (AG) and after 1 hour annealing (1h) to 115 hours annealing (115h). The increase of the graded layer peak intensity illustrates the interdiffusion process in the SL. Annealings were carried out at the growth temperature (800 °C) in an ammonia-based atmosphere. The color scale represents the logarithm of the diffracted intensity.

## Figure 2: single column

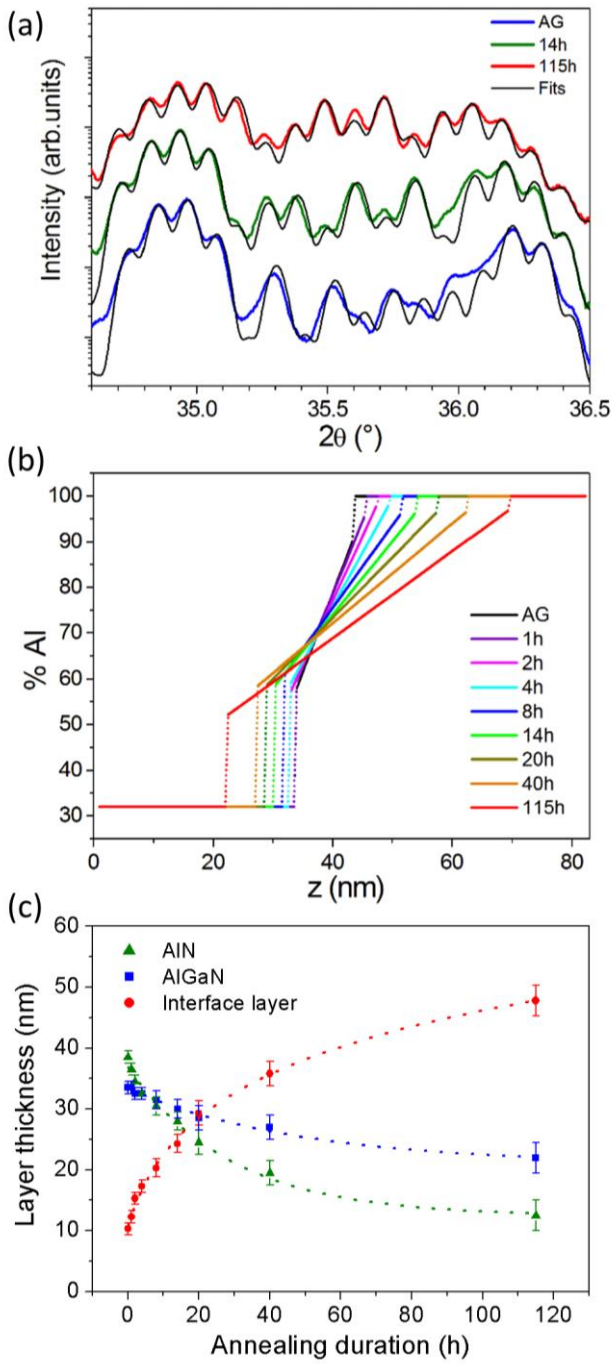


FIG. 2. (a) Measured *2θ-ω* scans of a 5-pair AlN/$Al_{0.3}Ga_{0.7}N$ superlattice for the as-grown sample (blue line), the 14-hour (green line) and the 115-hour (red line) annealing with the corresponding simulations (black lines). The curves have been arbitrary shifted. (b) Simulated aluminum content profile in the SL period of the as-grown and all the annealing samples from 1 to 115 hours. (c) The thickness evolution of the three layers of the SL period extracted from the XRD simulations.

## Figure 3: single column

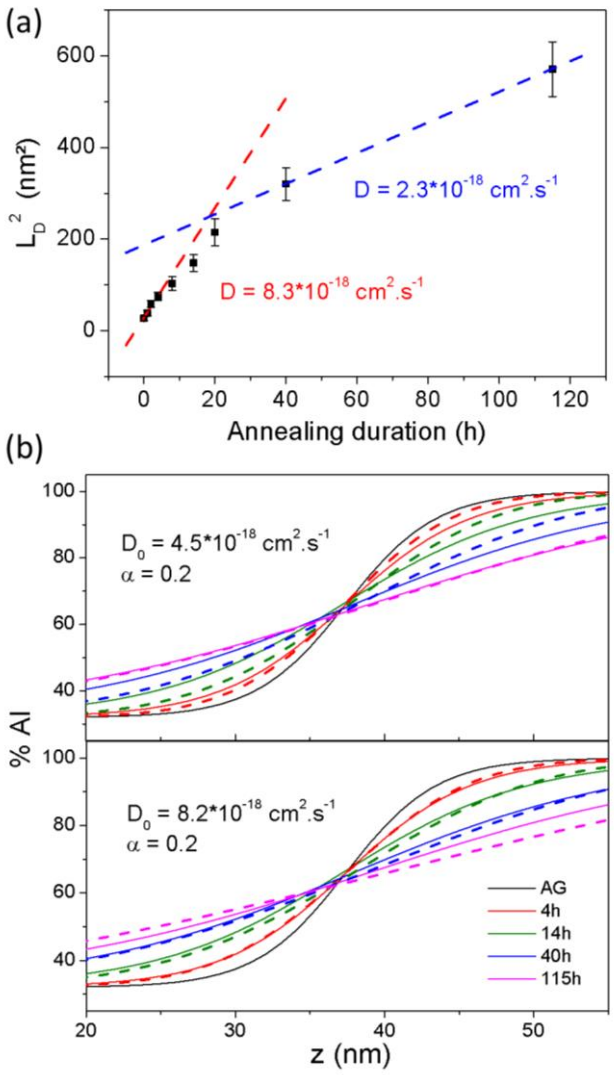


FIG. 3. Determination of the diffusion coefficient *D* at 800 °C in a 5-pair AlN/$Al_{0.3}Ga_{0.7}N$ superlattice. (a) In the case of a diffusion process only temperature-dependent, a unique value of *D(T=800 °C)* should be extracted from the slope of the squared diffusion length plotted against the annealing duration. (b) Considering this diffusion process to be temperature- and concentration-dependent in Fick's equation, a unique set of diffusion coefficient values ($D_0$, $\alpha$) should be extracted by comparing the sigmoidal fits of the XRD composition profiles (continuous lines) and the solutions of Fick's equation (dashed lines). The different $D_0$ values obtained after 4 hours (bottom graph) and 115 hours (upper graph) of annealing might mean that the diffusion is not only temperature and chemical concentration dependent.

## Figure 4: single column

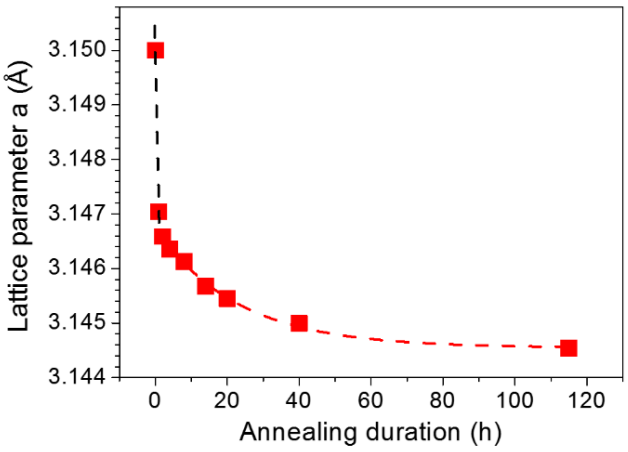


FIG. 4. In-plane lattice parameter variation against the annealing duration of a 5-pair AlN/$Al_{0.3}Ga_{0.7}N$ superlattice. The black dashed straight line highlights the drastic drop between the as-grown sample value and the 1h-annealed one. The red dashed line is an exponential fit decreasing from the 2h-annealing value to the 115h-annealing one.

## Figure 5: single column

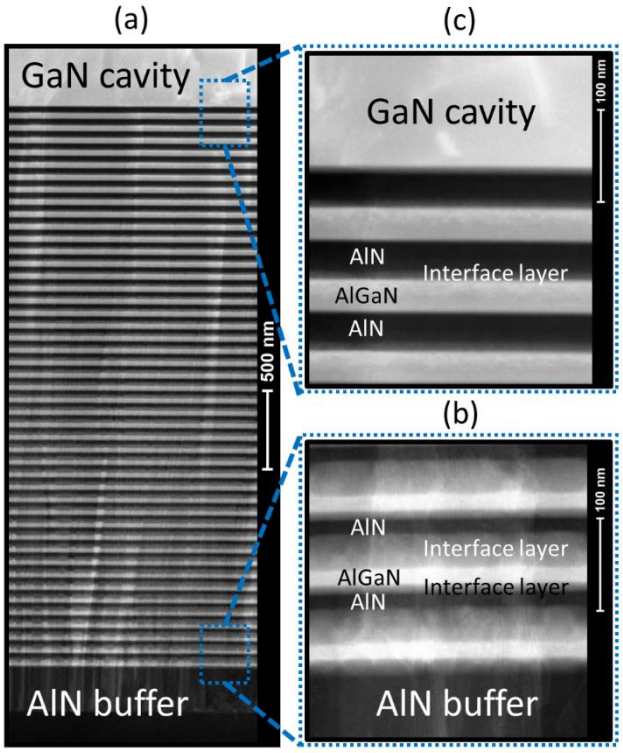


FIG. 5. (a) HAADF-STEM cross-sectional image showing an $(AlN/Al_{0.3}Ga_{0.7}N)_{45}$ DBR with interfaces sharper at the top than at the bottom of the DBR. This is confirmed at a magnified scale on (b) and (c). The first periods at the bottom of the DBR (b) show a four-layers stacking, for which the thickest layer is an interface layer at the AlN-on-AlGaN interface. A thinner second interface layer is also present at the AlGaN-on-AlN interface. The last periods at the top of the DBR (c) show a three-layers stacking with a thin interface layer at the AlN-on-AlGaN interface, whereas the AlGaN-on-AlN interface is sharper.

## Figure 6: single column

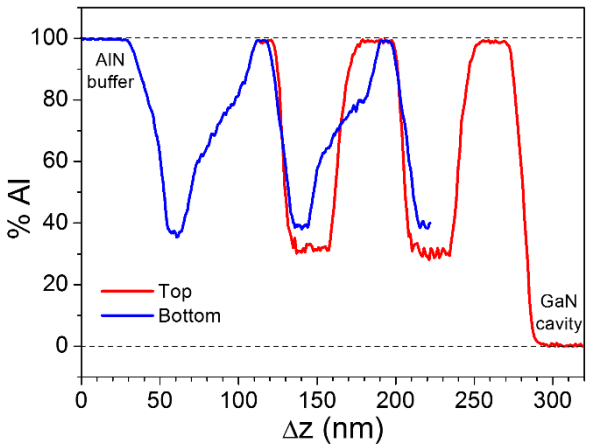


FIG. 6. Aluminum content profiles of an $(AlN/Al_{0.3}Ga_{0.7}N)_{45}$ DBR determined by EDX, on the sample cross section along the growth axis, at the bottommost (blue line) and the topmost (red line) DBR periods. For more clarity, the EDX profiles of the first two and the last two DBR periods have been superposed.

**Figure 7: 2 columns**

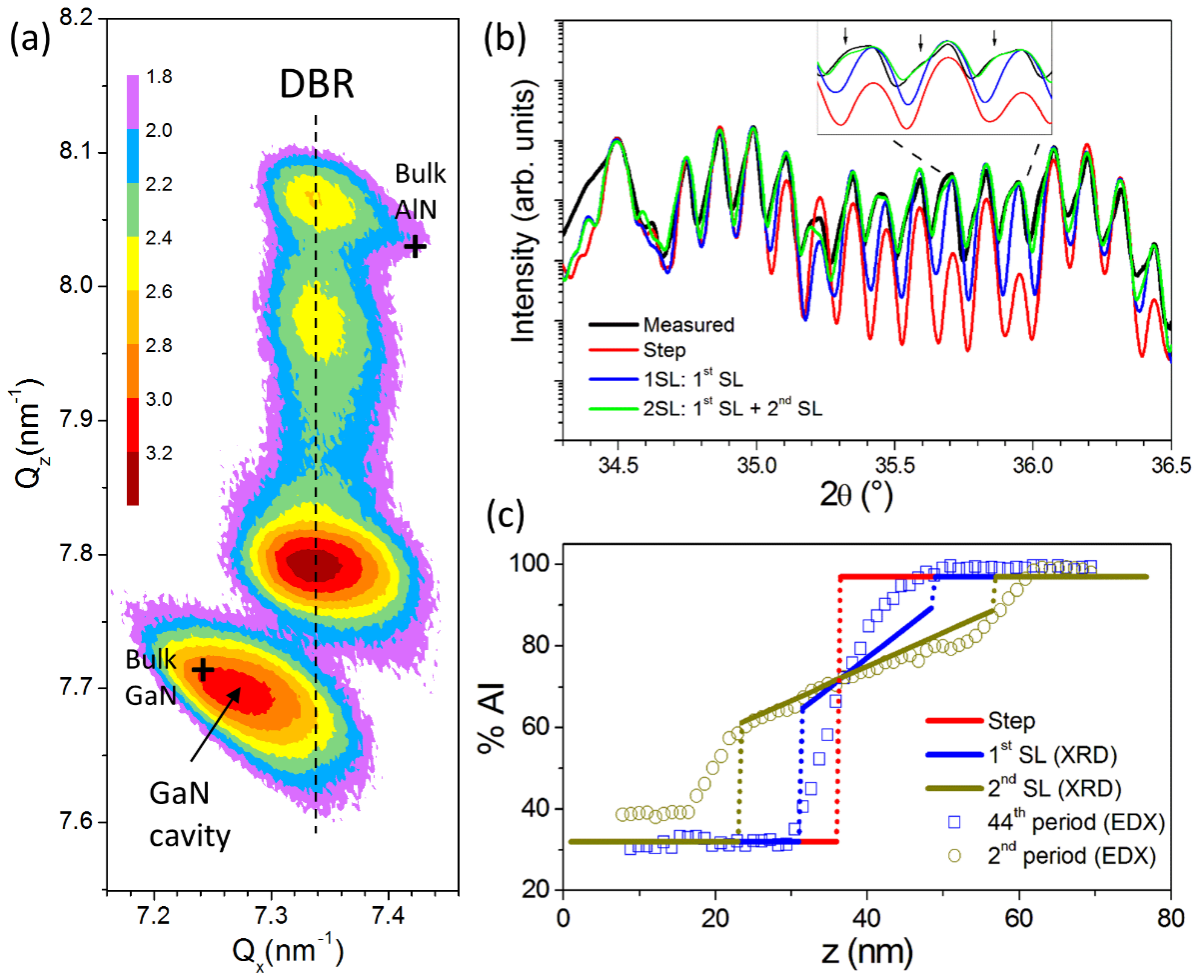


FIG. 7. (a) X-ray reciprocal space map of the $(20\bar{2}4)$ reflection of an $(AlN/Al_{0.3}Ga_{0.7}N)_{45}$ DBR (aligned peaks along the dashed black line) with a GaN cavity on top (bottom peak). The color scale corresponds to the logarithm of the diffracted intensity. (b) $2\theta$-$\omega$ scans of the (0002) reflection of the DBR. The black line corresponds to the measured diagram, the blue (resp. red) line corresponds to the simulated diagram with (resp. without) an interface layer in each period. The best simulation is obtained with two superlattices with different interface layer (green line). (c) Aluminum content profile in the period of the superlattice with (blue and dark yellow lines) and without (red line) interface layer. The profiles determined by EDX at the AlN/AlGaN interface of the 2$^{nd}$ (dark yellow circles) and the 44$^{th}$ (blue squares) periods of the DBR are reported for comparison.